

Fracture evolution in artificial bedded rocks containing a structural flaw under uniaxial compression



Ding-Jian Wang^{a,b}, Huiming Tang^{a,*}, Derek Elsworth^b, Chaoyi Wang^b

^a Department of Engineering Geology and Geotechnical Engineering, Faculty of Engineering, China University of Geosciences, Wuhan, Hubei 430074, China

^b Department of Energy and Mineral Engineering, EMS Energy Institute, and G3 Center, Pennsylvania State University, University Park, PA 16802, USA

ARTICLE INFO

Keywords:

Bedded rock
Bedding plane
Structural flaw
Crack propagation
Failure mode
Anisotropy

ABSTRACT

The Observation and prediction of crack propagation are important in understanding rock behavior in engineering practice. Previous studies have focused on homogeneous and isotropic rocks, but the influence of bedding planes on rock fracture is sparingly documented. In this study, we investigate the fracturing response in uniaxial compression of artificial bedded rocks containing variable-inclination bedding planes and single structural flaws. The recorded stress-strain data and captured cracking patterns are examined together. Nine separate crack types are identified in which bedding-plane sliding and splitting are potentially new. The presence of bedding planes plays a decisive role in crack propagation. With a steepening of the bedding plane, tensile cracks initiating from the structural flaw are better able to propagate along bedding planes, and the accumulative length of bedding fractures accordingly increases. Failure transforms from a purely tensile mode to a bedding sliding mode and subsequently to a bedding splitting mode as the bedding inclination increases. Compared to pro-dip flaw tests, the fracturing of bedding planes is triggered by both the tensile and shear stress with more far-field tensile cracks initiating from bedding planes in the specimens containing anti-dip flaws. Finally, the results are applied to predict the failure mode and fracture evolution in bedded rock slopes.

1. Introduction

Bedded rocks such as stratified sedimentary rocks and foliated metamorphic rocks are common in nature (Goodman 1989; Barton and Quadros 2015). They exhibit strong anisotropy in deformation, strength and failure mode due to their inherent (e.g. stratification, foliation, cleavage) and structural (e.g. joint, fault, fissure) discontinuities (Hoek and Bray 1981; Niandou et al. 1997; Cai and Kaiser 2004; Chen et al., 2008; Tang et al. 2017). These two types of discontinuities exert distinct effects on rock masses with respect to the evolution of deformability and rupture. Previous studies have mainly examined the role of inherent discontinuities (bedding planes) on response (Duveau et al., 1998; Gholami and Rasouli 2014; Togashi et al. 2017) but ignored the influence of structural discontinuities, or only examined the role of pre-existing flaws (Bobet and Einstein 1998; Wong and Einstein 2009a) in the absence of inherent discontinuities. However, the progressive failure of rock masses often results from crack propagation along a pre-existing defect; hence, it is crucial to study the cracking and failure processes of bedded rocks containing structural flaws.

Crack propagation leading to rock failure is of great significance for understanding the mechanical response of rock to external loads.

Numerous studies of crack propagation have been conducted on prismatic specimens containing single/several flaws. In accordance with the testing materials, flaw arrays and loading conditions, these studies can be summarized as: (1) Testing of various materials, including limestone (Feng et al. 2009), sandstone (Yang et al. 2013), marble (Zou and Wong 2014), granite (Yang and Huang 2017) and rock-like materials (Wong et al. 2001; Cao et al. 2015) to examine the resulting cracking behavior. (2) Designing of different flaw arrays, such as a single flaw (Zou et al. 2016), parallel and nonparallel flaw pairs (Wong and Einstein 2009b; Yang et al. 2013, 2017) and multiple flaws with different geometries (Yang et al. 2012; Cheng et al. 2015; Cao et al. 2016) to investigate their effects on crack initiation, propagation and coalescence. And (3) testing under different loading conditions- most experiments were conducted under uniaxial compression (Wong and Einstein 2009a, 2009b; Yang et al., 2017a, b) but some studies examined the complex loading paths of biaxial or triaxial experiments (Bobet and Einstein 1998; Yang and Huang 2017). In addition to the three aspects above, others have focused on the roles of size-effects and shape-effects on specimens/discontinuities (Bandis et al., 1981; Indelicato and Paggi, 2008; Carpinteri and Paggi, 2008; Song et al., 2018). Besides, certain new techniques such as high-speed

* Corresponding author.

E-mail address: tanghm@cug.edu.cn (H. Tang).

<https://doi.org/10.1016/j.enggeo.2019.01.011>

Received 5 August 2018; Received in revised form 7 January 2019; Accepted 15 January 2019

Available online 18 January 2019

0013-7952/ © 2019 Published by Elsevier B.V.

photography, image processing, acoustic emission monitoring, X-ray and CT imaging were utilized in recent studies to define the evolution of fracturing (Wong and Einstein 2009c; Yang et al. 2012, 2013). These experimental studies contribute to our fundamental knowledge of crack propagation within rocks.

A recent study of fracture evolution in Opalinus shale (Morgan and Einstein 2017) shows that cracks initiating at flaw tips usually propagate along bedding planes and this mode further dominates as the bedding planes become steeper. However, most studies to date have ignored the role of bedding and focused solely on homogeneous and isotropic specimens. The influence of heterogeneities, such as bedding planes, on the cracking process is very sparingly documented. Therefore, further studies are required to reveal the mechanisms of fracture evolution in bedded rocks containing various structural flaw arrays.

We present the observations of fracture evolution in artificial bedded rocks containing single structural flaws under uniaxial compression. We analyze the stress-strain response to define how the effective mechanical parameters vary with specimen and flaw geometries. Through the cracking patterns captured by the video camera, we identify the crack types initiating in each specimen and investigate the effects of the bedding plane and structural flaw on crack propagation.

2. Specimen preparation and testing procedure

Experiments are conducted on anisotropic prismatic specimens containing a structural flaw. To maintain consistency in the results, the specimens are rigorously prepared according to a uniform protocol.

2.1. Specimen preparation

Artificial rocks are widely used to study the evolution of fracture and other aspects of the mechanical response as analogs to real rocks (Wong et al. 2001; Tien et al. 2006). The principal benefits of analogs are that structure and properties may be controlled and that multiple replicates of experiments may therefore be completed. In this work, the behavior of bedded specimens containing a structural flaw is examined through controlled experiments with variable inclinations of bedding and flaw configurations. The rock-like material is a mixture of cement, sand, calcium bentonite and water at a ratio of 6:3:1:3.48 and cured at 20 °C and relative humidity (RH) > 90%. Silicate cement of grade 42.5 (i.e., UCS \geq 42.5 MPa) is used as gelatinizer. The grain sizes of the sand and calcium-bentonite are 0.075–0.3 mm and < 0.075 mm, respectively. Specimen preparation follows the four steps below and is also illustrated in Fig. 1(a):

Step 1: Mix the ingredients of the composite material. The pre-weighed ingredients are well blended and then poured into a hollow cuboid vessel in a dimension of 30 × 20 × 20 cm. The mixed slurry is then well shaken using a vibrating table (1 Hz frequency and for 300 s) to remove any remaining air bubbles.

Step 2: Make the bedding planes by cutting with steel wires. The blended mixture cures as a gel after standing for 200 min. Three sides of the vessel are disassembled to expose the inner curing material. Then, the material is horizontally cut using equidistant wires (Fig. 1(b)). This process leaves a bedded structure with equal layer thickness of 10 mm.

Step 3: Cure the bedded mass at 20 °C, RH > 90% for 28 days to ensure complete hydration cement. The bedded mass is then air-dried to remove the internal moisture.

Step 4: Cut into designed specimens. First, the cured bedded chunk is cut into several standard prismatic blocks for uniaxial compression tests with a uniform dimension of 142 × 72 × 40 mm. Then, a throughgoing flaw is cut in each specimen by high-pressure water-jet (Fig. 1(c)). The length and width of the flaw are 20 mm and 2 mm, respectively. Fig. 1(d) shows all 34 specimens with various bedding and flaw inclinations.

The machines/tools used for making specimens have a high degree of accuracy. All the specimens are manufactured under the uniform

standard and cured under the same condition; hence, the properties of bedding planes in the same specimens and among different specimens are similar.

2.2. Geometries of the specimen and flaw

The prismatic specimen measures 142(height) × 72(width) × 40(thickness) mm (Fig. 2). Three geometric parameters are defined to characterize a structural flaw in the bedded specimen: the bedding inclination α , flaw inclination β and flaw length L . To examine the effects of bedding and flaw inclinations on crack propagation, we maintain L constant at 20 mm for all specimens but assign different values to α and β . Here, α has five different values, and β has eight values as noted in Table 1. In terms of their inclinations, there are four types of flaws, viz., horizontal, vertical, pro-dip ($0^\circ < \beta < 90^\circ$) and anti-dip ($-90^\circ < \beta < 0^\circ$) flaws. The mnemonic $S\alpha\beta$ defines a particular specimen where S represents the structural flaw and α and β indicate the inclinations of bedding and flaw relative to the horizontal. For the anti-dip flaw with a negative β value, 'minus' will be substituted by 'm'. Parametric analysis is conducted by changing one of the two parameters while keeping the other constant.

2.3. Testing procedure

The testing system comprises two parts - uniaxial compression testing apparatus and data acquisition, as shown in Fig. 3(a). In this study, the loading rate is displacement-controlled at 0.002 mm/s. During the loading process, the rock deformation is recorded continuously via a video camera (Fig. 3(b)) together with the stress-strain data. The rate of the video camera is up to 59.94 frames per second and the maximum resolution of a single frame is 1920 × 1080 pixels. The recorded images and data are combined to analyze fracturing process in the artificial bedded rocks.

3. Results: deformation and strength behaviors

The Recorded stress - strain data are described in detail and further analyzed to define the evolution of mechanical response of the specimens.

3.1. Stress-strain relationships

Axial stress-strain curves of all 34 specimens are plotted in groups with respect to the bedding inclination, as shown in Fig. 4. Each stress-strain curve is characterized by four phases, regardless of the bedding or flaw inclination: the initial nonlinear phase, linear elastic phase, plastic-failure phase, and post-failure phase (Fig. 5(a)). The initial nonlinear phase indicates a response to the closure of inherent pores within the specimens. The linear elastic phase indicates the deformation of the particle within rock and the steady development of micro-cracks. The onset of the plastic-failure phase is marked by the formation of macro-cracks. As soon as the peak strength is attained, the axial stress drops, typically in several steps, until the residual strength is reached.

From these four phases of the stress-strain curves identified above, four types of stress-strain relationships are generalized - ductile with fluctuation (type A), ductile without post-peak fluctuation (type B), brittle failure with fluctuation (type C) and brittle failure without post-peak fluctuation (type D), as illustrated in Fig. 5(a). In the first two phases (I and II), no apparent differences are observed among the four types. However, from the beginning of phase III, both the type A and B show a broad transitional zone that crosses over the peak strength and stretches to phase IV, indicating a ductile failure mode. The post-peak trend of type A is accompanied by fluctuations in the strength. Types C and D are marked by a steep drop in the stress at the peak, typically indicating a brittle failure. Types C and D are distinguished from each other by whether the post-peak reduction in strength is either steady

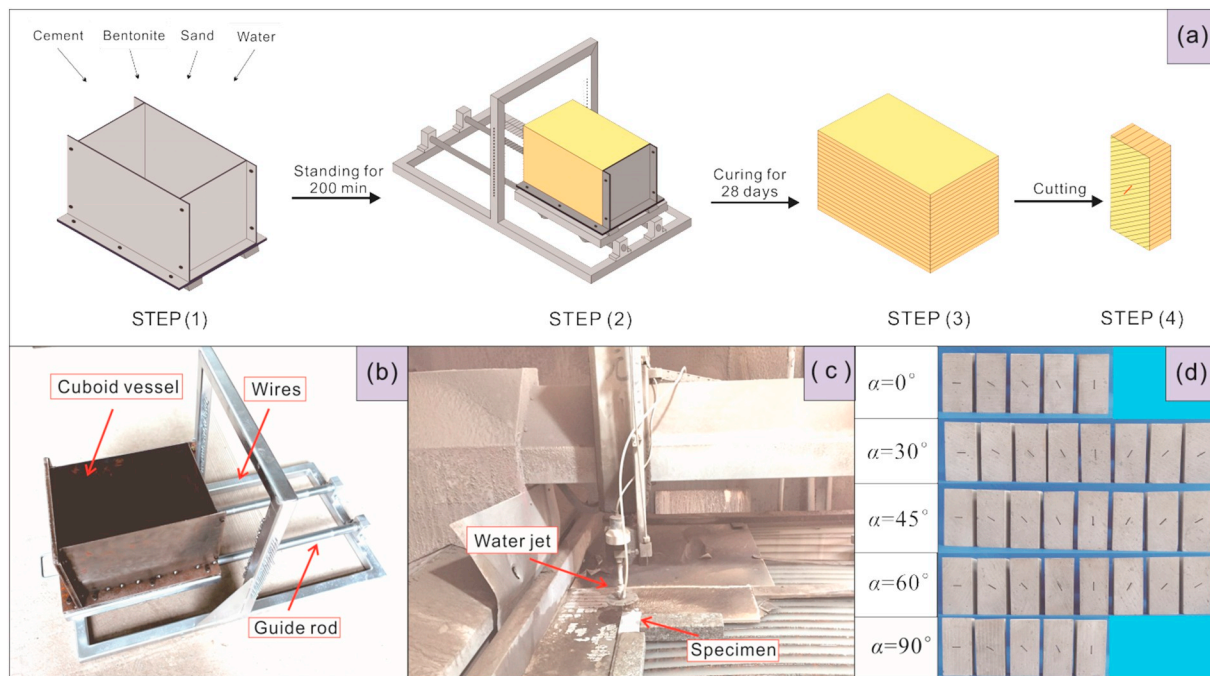


Fig. 1. (a) Sequence of procedures for specimen preparation. (b) Photo of slicing apparatus for introducing bedding planes and prosmatic vessel for holding the mixed materials. (c) Photo of high-pressure water jet. (d) Prepared bedded specimens containing single structural flaws.

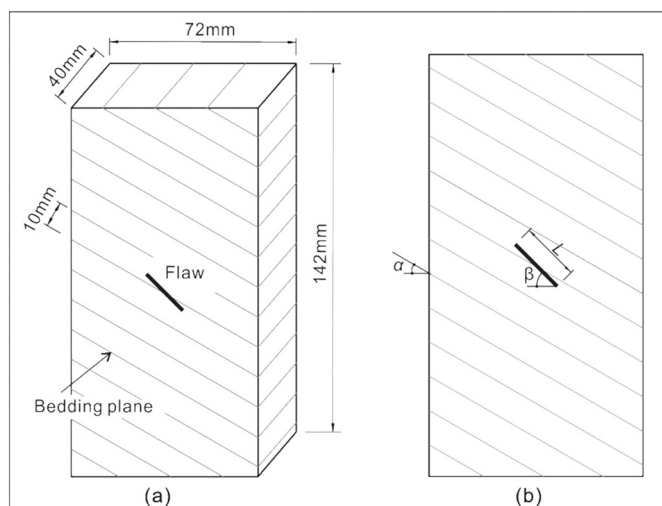


Fig. 2. Geometry of the single structural flaw within a bedded specimen: (a) 3-dimensional view; (b) 2-dimensional view.

Table 1
Inclinations of bedding and flaw of all the prepared specimens.

Series	Bedding inclination α (°)	Flaw inclination β (°)
S0- β	0	0, 30, 45, 60, 90
S30- β	30	0, 30, 45, 60, 90, -60, -45, -30
S45- β	45	0, 30, 45, 60, 90, -60, -45, -30
S60- β	60	0, 30, 45, 60, 90, -60, -45, -30
S90- β	90	0, 30, 45, 60, 90

(D) or fluctuating (C). In accordance with the experimental results, Fig. 5(b) shows the specific curve types of specimens with different bedding and flaw inclinations.

3.2. Mechanical parameters

In the present study, three key parameters are defined in evaluating the mechanical behavior of rock - the uniaxial compressive strength (σ_c), uniaxial strain at peak stress (ϵ_c) and elastic modulus (E). Anisotropy in the mechanical parameters is pronounced, resulting from the dual presence of bedding planes and structural flaw.

The uniaxial compressive strength varies with the bedding and flaw inclination, as illustrated in the polar plots of Fig. 6. The radial and circular ordinates of the polar plot represent values of both the bedding and flaw inclinations, respectively. Hence, the variation in the uniaxial compressive strength determined by the various specimen geometries is reflected in a 2-dimensional plane. As the bedding plane steepens, σ_c appears to first decrease and then increase. Retaining β constant, the minimum and maximum values of σ_c are recovered for $\alpha=60^\circ$ and 90° , respectively. The two poles in the polar plot indicate that the strength of specimens with $\beta= -30^\circ$ and 45° are the weakest.

The uniaxial strain at the peak stress denotes where the peak stress is attained. Fig. 7 illustrates the variation in the uniaxial strain at the peak stress as functions of the bedding and flaw inclinations. The trough surrounding the circle center indicates that the magnitudes of ϵ_c are the minimum when α approaches 60° . Also, the ϵ_c values of the specimens containing pro-dip flaws are lower than those of the specimens containing anti-dip flaws.

The elastic modulus is a critical parameter in evaluating mechanical properties in the early stages of deformation and can be measured from the slope of the linear elastic phase of the stress-strain curve. The modulus of the specimens with different geometries is shown in Fig. 8. The value of E first decreases and then increases as β varies from -90° to 90° . The minimum value is attained with β between -45° and 45° . It is also apparent that E has a positive relation with α in general.

4. Results: cracking behavior

The entire cracking process of the artificial bedded rocks under uniaxial compression are recorded and visualized by the video camera. The crack types and failure modes can be further identified from the observed evolving crack patterns.

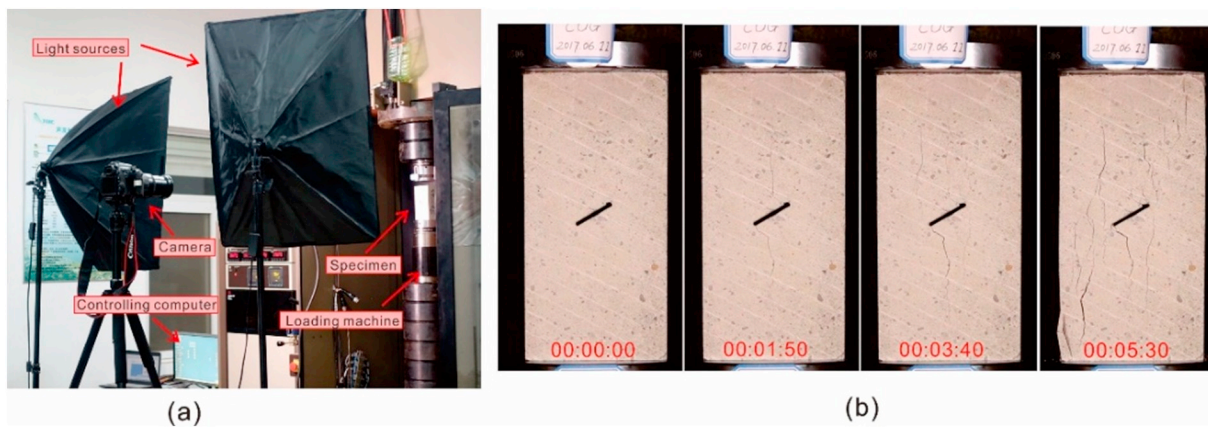


Fig. 3. (a) Uniaxial compression machine and recording system. (b) Images at different stages in the entire loading process.

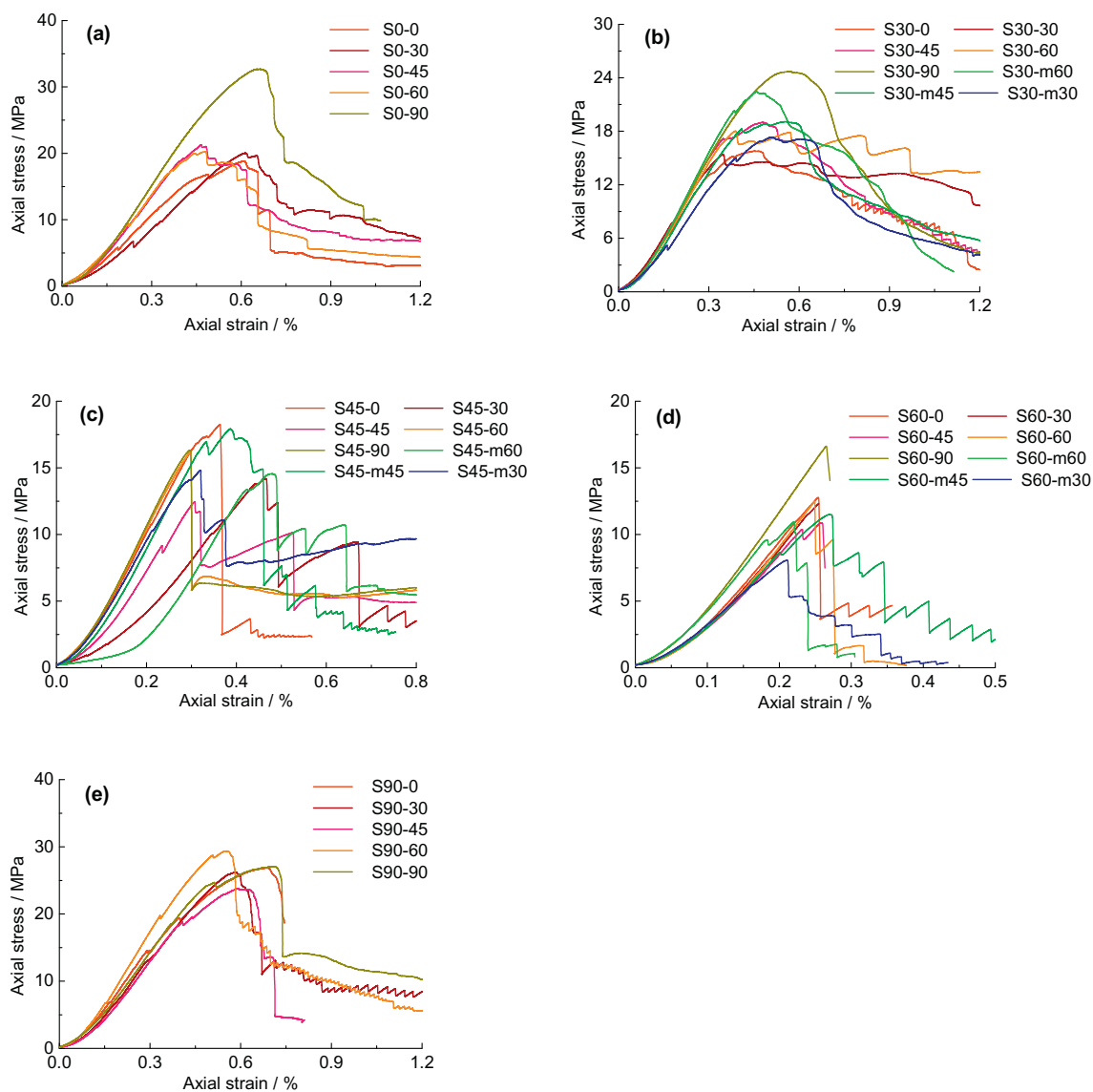


Fig. 4. Axial stress-strain curves of bedded rocks containing single flaws: (a) $\alpha = 0^\circ$, (b) $\alpha = 30^\circ$, (c) $\alpha = 45^\circ$, (d) $\alpha = 60^\circ$, (e) $\alpha = 90^\circ$ (e.g. ‘m’ is ‘minus’ in short, indicating the specimen contains anti-dip flaw).

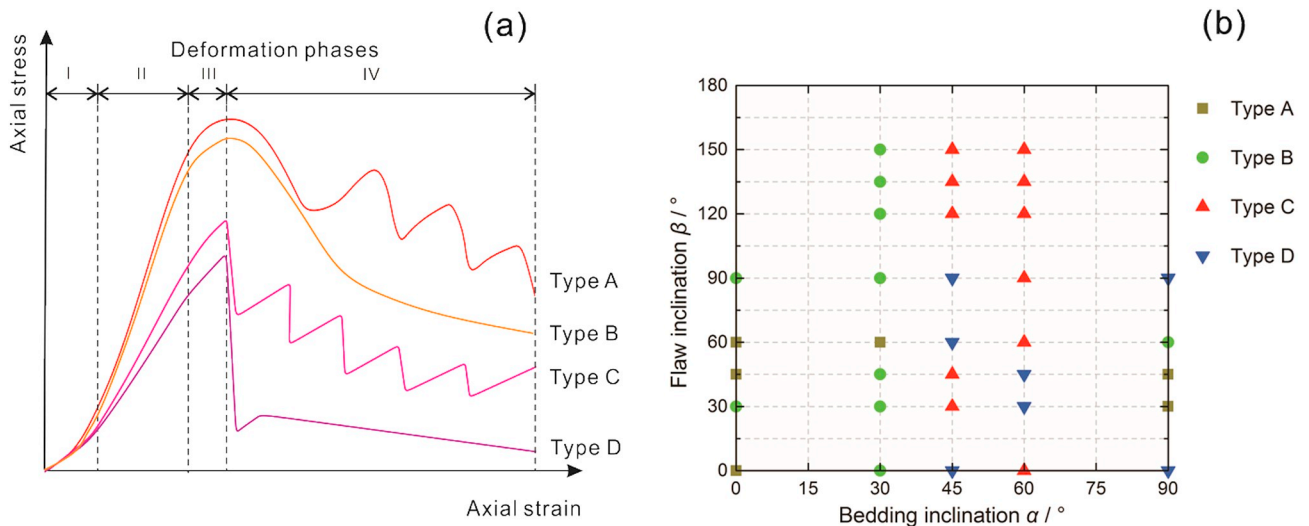


Fig. 5. (a) Deformation phases and types of stress-strain curves. (b) Curve types corresponding to specimens with different geometries.

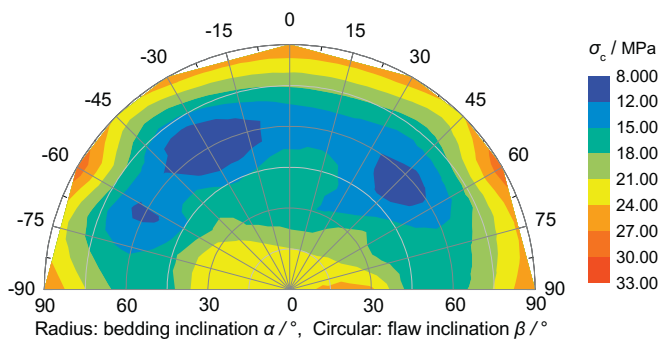


Fig. 6. Uniaxial compressive strength varying with bedding and flaw inclinations.

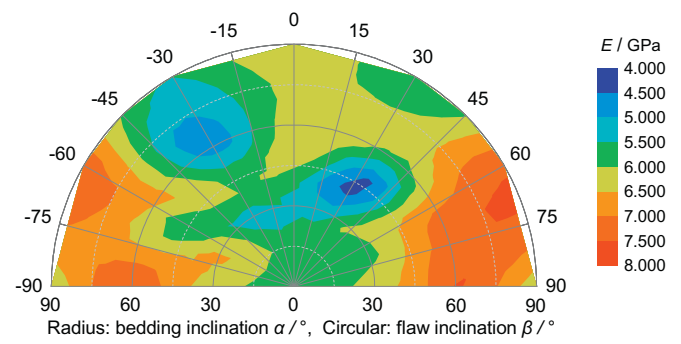


Fig. 8. Elastic modulus varying with bedding and flaw inclinations.

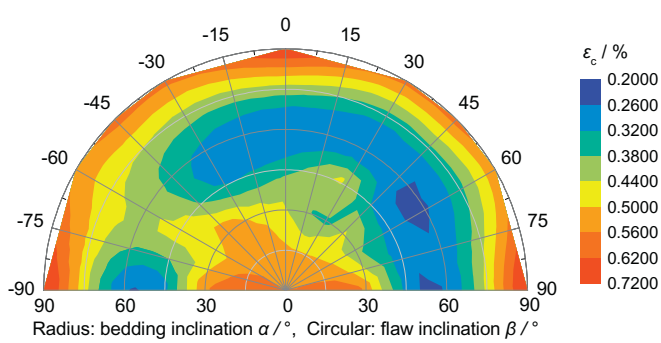


Fig. 7. Uniaxial strain at peak stress varying with bedding and flaw inclinations.

4.1. Crack types

In light of internal mechanism and geometries of the observed cracks, nine different crack types are identified as shown in Fig. 9. Characteristics of each crack type are presented in Table 2 and described in detail below.

Tensile wing crack (T_w): The wing crack initiates at the flaw tip or at a certain distance away from the tip. The crack propagates toward the end of specimen with the direction rotating parallel to the direction of axial loading. The wing crack appears in two forms with different initiating directions: form 1 follows the flaw extension while form 2 propagates in the opposite direction.

Tensile vertical crack (T_v): This crack type also initiates from the flaw tip or a certain distance from it and extends parallel to the direction of axial loading. The tensile vertical crack usually appears after a wing crack has developed.

Anti-tensile crack (T_a): The crack path is of similar trajectory to T_w and T_v, but its direction of propagation is the reverse - hence this type of crack is called an anti-tensile crack (Yang and Jing 2011).

Tensile-shear crack (TS): The crack initiates at the flaw tip and primarily follows a similar path to that of T_v. However, due to the impact of shear stress, the path gradually rotates and propagates at an angle of 45° relative to the direction of axial loading as it approaches the specimen end.

Shear-tensile crack (ST): The crack primarily initiates along the flaw direction, and then gradually rotates to be parallel to the direction of axial loading. Although of similar shape to the ‘form 2’ tensile wing crack, the shear-tensile crack is initially triggered by shear stress but is finally constrained by tensile stress.

Shear crack (S): The crack initiates at the flaw tip, and propagates along the direction of the flaw. It is approximately coplanar or oblique to the structural flaw.

Far-field crack (F_t and F_s): The far-field crack has two forms: a far-field tensile crack (F_t) and a far-field shear crack. They both initiate remotely from the flaw tip and develop along a non-planar path.

Shear sliding along bedding plane (S_b): The bedding-plane sliding propagates along the bedding plane but remotely from the flaw when the flaw inclination is shallow. In most cases, the bedding-plane sliding occurs as a stepped form with interlayer tensile cracks.

Axial splitting along bedding planes (S_p): The bedding-plane splitting initiates as a tensile crack propagating along the bedding plane. This

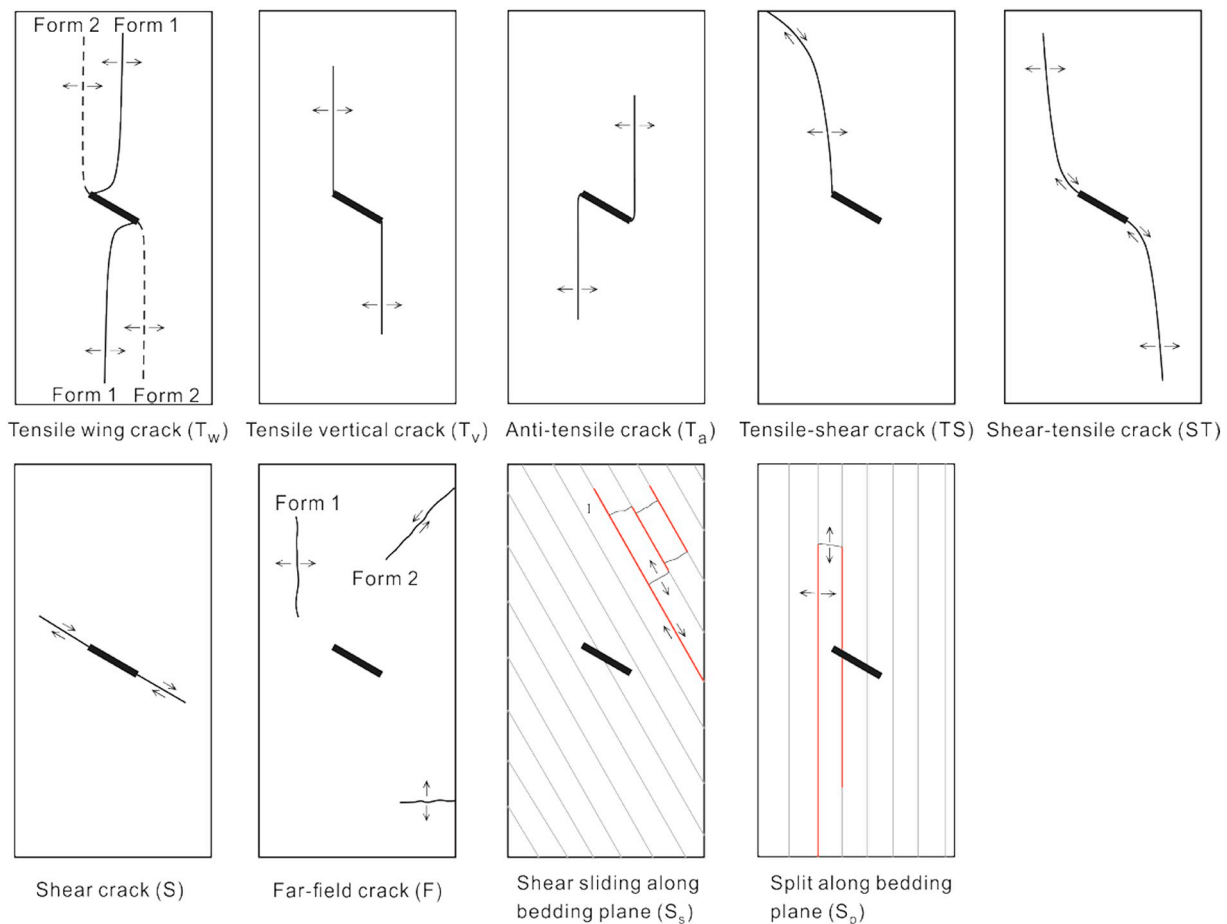


Fig. 9. Crack types initiating in bedded specimens containing single flaws.

type of crack predominates in specimens with vertical bedding planes. Some tensile cracks will simultaneously occur at the top of the failed layer due to the effect of buckling.

The use of the above classification of crack types lies in describing processes that dominate under different conditions of the bedding and flaw orientations relative to the loading. The experimental results show that the fracturing processes in bedded rock are controlled by the presence of bedding planes and structural flaws and involve various crack types which combine in different sequential and spatial forms. Table 3 summarizes the crack types observed in each specimen.

4.2. Failure modes

Investigating failure modes in rock is largely driven by the motivation of engineering characterization of the performance of structures on and in rock. The failure mechanisms of artificial bedded rocks containing single structural flaws can be classified into five modes, namely, tensile failure, combined tensile-shear failure, combined tensile-bedding sliding failure, bedding sliding failure and splitting failure.

Tensile failure: coalescence of tensile cracks leads to the failure of the specimen. This mode of failure is uncommon and mostly occurs in specimens containing horizontal bedding planes.

Combined tensile-shear failure: This failure mode occurs as a tensile crack in the initial stage eventually transforms to a shear crack, or the inverse transformation occurs. This mode is likely in specimens with a shallow inclination of the bedding ($\beta \leq 30^\circ$).

Combined tensile-bedding sliding failure: This failure mode is a combination of tensile failure and bedding sliding failure. It is observed in such specimens only when the bedding inclination ranges from 30° to 60° and the flaw inclination is greater than -60° or lower than 30° .

Bedding sliding failure: The Bedding sliding is induced by shear stress. This failure mode is separately classified as a new mode to distinguish it from general shear failure. Compared to the combined tensile-bedding sliding failure, this mode is dominated by bedding-plane sliding and is barely affected by tensile cracks. A prerequisite to bedding sliding failure is that the bedding and flaw inclinations lie between 45° to 60° and 30° to 90° , respectively.

Splitting failure: This failure mode is triggered by the splitting of bedding planes and the bending of the strata. All specimens with vertical bedding respond in this mode.

The failure modes dominated by bedding and flaw inclinations are plotted in β - α coordinates, as shown in Fig. 10. In general, the failure transforms from the purely tensile mode to the bedding sliding mode and subsequently to the bedding splitting mode following the order above as bedding inclination increases.

The relation of the failure mode to uniaxial compressive strength is illustrated in Fig. 11, with a single failure mode occurring in multiple specimens with different geometries. The average strength for each mode is also presented for comparison. The specimens failing in the bedding-plane sliding mode are weakest, and those failing in the bedding splitting mode are strongest. In addition, the strengths of specimens with tensile failure and combined tensile-shear failure are situated at the mid-level, but the latter one exhibited a higher discretization.

5. Discussion and implication

5.1. Comparison to homogeneous rock tests

Previous studies involving crack propagation have been conducted

Table 2
Characteristics of identified crack types.

Crack type	Initiation point	Path	Mechanism	Feature
Tensile wing crack	Flaw	Propagating from flaw to specimen end	Tensile stress	Appearing as wing shape
Tensile vertical crack	Flaw	Propagating from flaw to specimen end	Tensile stress	Vertically propagating along axial loading direction
Tensile-shear crack	Flaw	Vertical in primary stage, transforming to be inclined eventually	Initially tensile stress, then shear stress	The shear part of the crack generally consists of smallish sub-cracks, which appears to be a shear band
Shear-tensile crack	Flaw tip	Initially propagating along flaw direction, then transforming to vertical path	Initially shear stress, then tensile stress	The shear part of the crack appears as a cambered shape
Shear crack	Flaw tip	Inclined path extending to boundary	Shear stress	Mostly shown as an en-echelon form
Far-field crack	Away from flaw	Running through specimen	Tensile stress or shear stress	Developing away from the flaw but usually coalescing with other cracks
Bedding-plane sliding crack	Flaw, bedding plane or preformative crack	Along bedding plane	Shear stress	Appearing to be the extension of preformative crack or fracture of the whole bedding plane
Bedding-plane splitting crack	Flaw, bedding plane or preformative crack	Along bedding plane	Tensile stress	Splitting of the whole bedding plane with smallish tensile crack concomitant on the top

Table 3
Summary of all crack types observed in the bedded specimens containing single flaws.

Series	T _w	T _v	T _a	TS	ST	S	S _s	S _p	F _t	F _s
S0-0	●	○		○					○	
S0-30	●		○		○				○	
S0-45	●	○	○		○	○			○	
S0-60	●		○		●				○	○
S0-90	●	○				●			●	●
S30-0	●				○	○				
S30-30	●	○			○	○	○		○	
S30-45	●				○	○	○			
S30-60	●		○			○	○			
S30-90	●	●				●	○		○	
S30-m60	●			○			○		○	○
S30-m45	●		○		○	○	○		○	
S30-m30	●	○	○			○	○		○	
S45-0	●	●					○		○	
S45-30	●		○				○		○	
S45-45	●		○				○		○	
S45-60	●						○		○	
S45-90	●	●					○		○	
S45-m60	●						○		○	
S45-m45	●	○					○		○	
S45-m30	●	○					○		○	
S60-0	●						●		●	
S60-30	●						●		○	
S60-45	●		○				○			
S60-60	●						○			
S60-90	●						●		○	
S60-m60	●						○		○	
S60-m45	●				○		○		○	
S60-m30	●						○		○	
S90-0	●							●	○	
S90-30	●		○					●	○	○
S90-45	○							●		
S90-60								●	○	
S90-90		●	○					●	○	

● indicates the crack is the primary crack to initiate, and ○ represents the non-primary initiating crack.

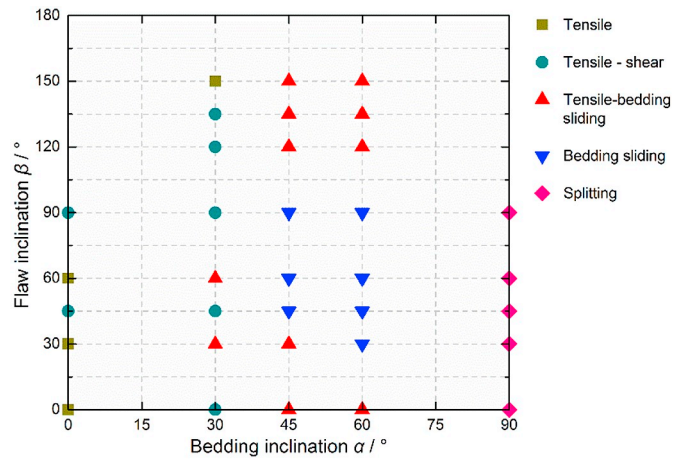


Fig. 10. Failure modes corresponding to specimens with different geometries.

on several types of rocks (e.g. marble, sandstone, granite, gypsum, etc.) which were mostly homogeneous. This study explores artificial bedded rocks containing single structural flaws and the results are compared to previous research on homogeneous rocks as follows.

5.1.1. New crack types

Seven crack types including three tensile cracks, three shear cracks and one mixed tensile-shear crack were observed in marble and gypsum (Fig. 12(a)) (Wong and Einstein, 2009a). The far-field crack and surface spalling were also added to the crack classification in sandstone

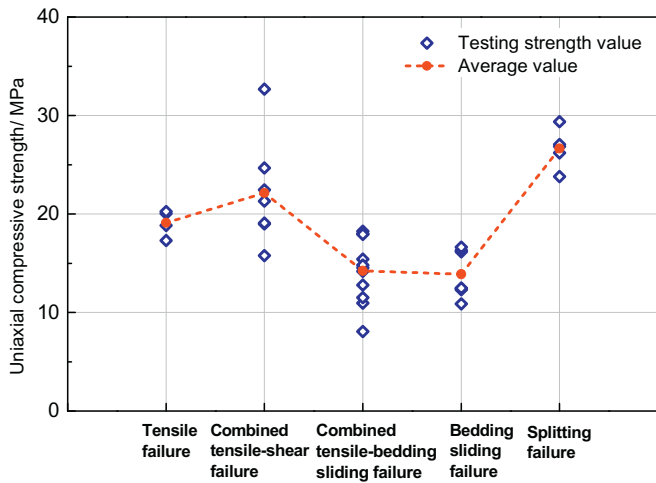


Fig. 11. Uniaxial compressive strengths of specimens subjected to different failure modes.

(Fig. 12(b)) (Yang and Jing 2011) in addition to the common tensile and shear cracks. Compared to previous testing results of homogeneous rocks, two new crack types are provisionally observed in this study - namely, bedding-plane sliding and bedding-plane splitting. These two crack types are specifically related to the presence of bedding planes which are significantly weaker than the rock matrix. A steeper inclination of the bedding planes enhances the generation of these two types of cracks.

5.1.2. Cracking paths

A comparison of the cracking paths between the current and previous studies is illustrated in Fig. 13. In homogeneous rocks (e.g. sandstone and marble), the crack propagates smoothly under the action of external pressure. However, in bedded rocks, the cracking paths are irregular and comprise multiple connected branches. Sharp transitions in the cracking direction are observed along the bedding planes as a crack approaches (Fig. 13(a)). These transitions were not observed in the homogeneous samples, such as sandstone and gypsum (Fig. 13(b) and (c)). The mechanism for this phenomenon may be due to the high

degree of stress concentration resulting between bedding planes where the cracking direction abruptly changes to release stress as the crack propagates near a bedding plane.

5.2. Effects of bedding planes

5.2.1. Crack initiation

Tensile cracks are the predominant crack types to primarily initiate under uniaxial compression. The tensile wing cracks are frequently observed as the primary crack in approximately 80% of all specimens. It is worth noting that the bedded specimens those do not primarily feature tensile wing cracks all possess a bedding or flaw inclination of $\alpha = 90^\circ$ or $\beta = 90^\circ$. Bedding-plane sliding and splitting modes also develop as the primary crack, particularly for specimens with steep bedding planes. The former primarily initiates in specimens with $\alpha = 60^\circ$ while the latter occurs in those with $\alpha = 90^\circ$. In addition, the primary cracks usually co-develop with two or more types combined in several specimens, reaching a percentage of approximately 30%. This phenomenon is particularly apparent when bedding planes are steep.

The threshold stress for crack initiation is a key parameter with respect to engineering applications. The normalized initiation stress R_i is herein introduced, which is defined as the ratio of the initiation stress relative to the uniaxial strength. The influence of α and β on R_i is intuitively revealed in Fig. 14 and which can be divided into three parts. First, when $-90^\circ < \beta < -45^\circ$, the value of R_i gradually decreases as the bedding planes become steeper. Second, as $-45^\circ < \beta < 45^\circ$, the maximum and minimum values of R_i are attained when $\alpha = 60^\circ$ and 30° , respectively. Third, as $45^\circ < \beta < 90^\circ$, the varying trend of R_i is similar to the first part, but the level of R_i is much higher. Of critical interest are cases with large R_i in engineering practice for which the progression from crack initiation to rock failure is particularly abrupt.

5.2.2. Crack propagation

In bedded rocks, tensile cracks initiating from structural flaws gradually tend to propagate along bedding planes under continuous loading (as shown in Fig. 15(a)). This effect is enhanced as bedding planes become steeper. It is common that bedding fractures are arranged in a stepped form with small tensile cracks that cut-across various strata (Fig. 15(b)), specifically when $\alpha = 30\sim 45^\circ$. Eventually, as α approaches 90° , the failure mode of the bedding planes transforms

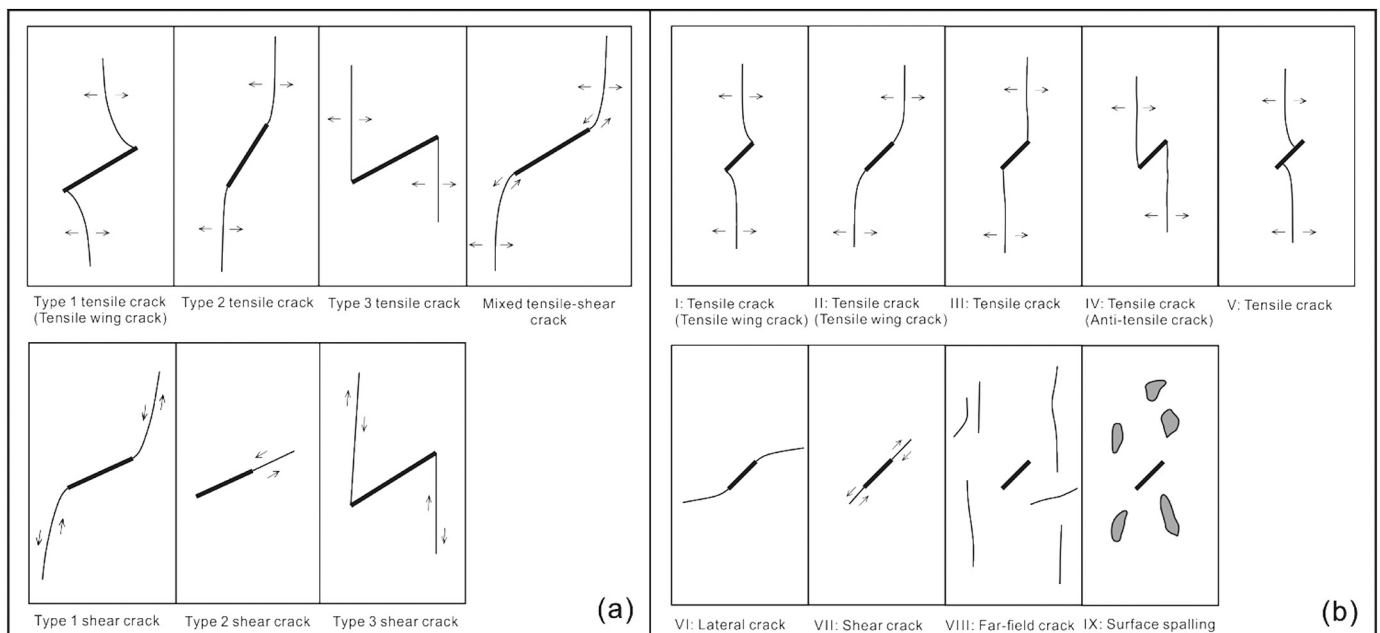


Fig. 12. Crack types identified from uniaxial compression tests on (a) marble by Wong and Einstein (2009a) and (b) sandstone by Yang and Jing (2011).

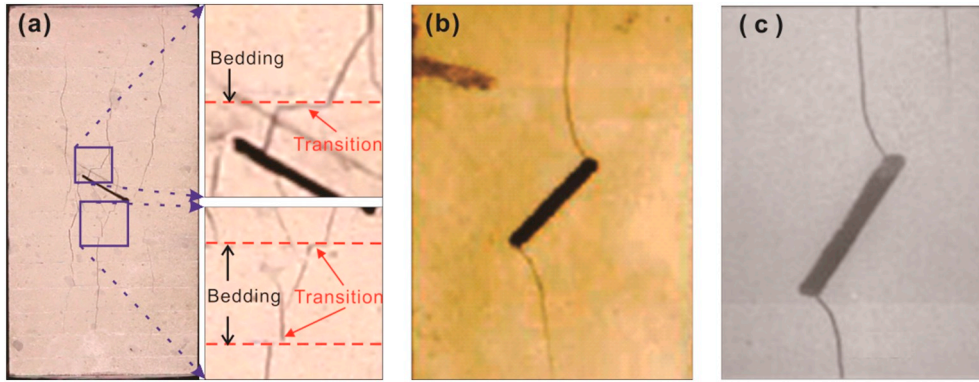


Fig. 13. Comparison of the cracking paths of bedded rock to homogenous rock tests: (a) artificial bedded rock, (b) sandstone (Yang and Jing 2011) and (c) gypsum (Wong 2008).

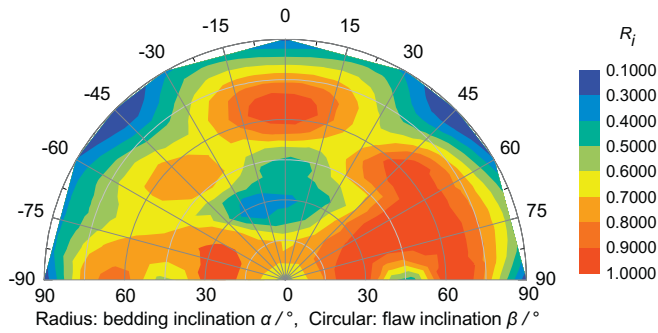


Fig. 14. R_i value varying with bedding and flaw inclinations.

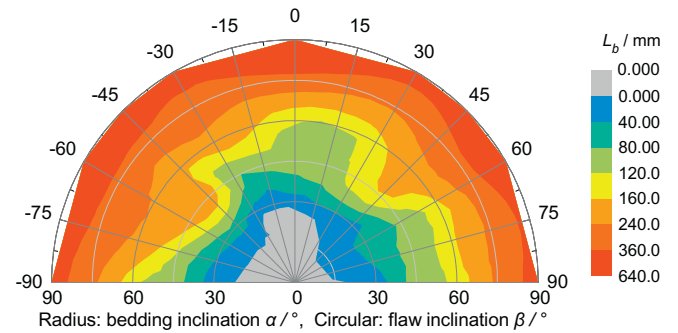


Fig. 16. Accumulative length of fractured bedding planes varying with bedding and flaw inclinations.

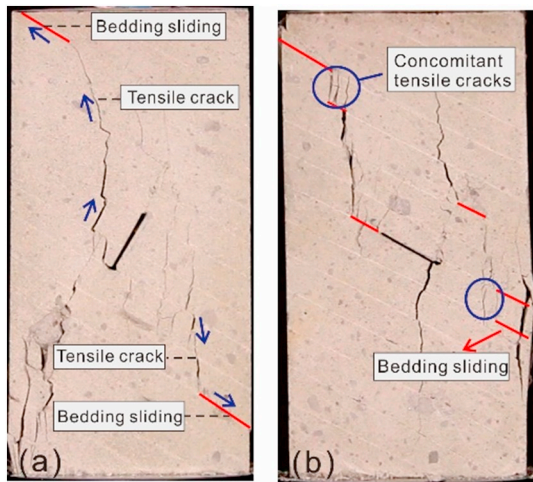


Fig. 15. (a) Evolution of the tensile cracks initiating from flaw (S30–120 for example). (b) Sketch of stepped bedding fractures and concomitant tensile cracks (S30–30 for example).

from sliding to splitting and tensile cracks are distributed throughout the splitting strata.

To reveal the influences of the bedding inclination on crack propagation, the accumulative lengths of bedding fractures (L_b) are calculated and plotted in Fig. 16. It is clear that L_b is positively related to α regardless of the variation in the flaw inclination, indicating that bedding fracture is more likely to develop in steeply-bedded specimens.

5.3. Comparison of pro-dip and anti-dip flaw tests

Pro-dip and anti-dip flaws are two common forms of defects in bedded rocks. It can be concluded from the experimental results that

these two flaw forms exert distinct and definable influences on the sequence of crack formation and failure mode of artificial bedded rocks.

For specimens containing pro-dip flaws, bedding-plane sliding fractures coalesce with the tensile cracks that initiate from the structural flaw, ultimately leading to the failure of rock. This result is possibly due to the fact that the pro-dip flaw appears to be conducive to bedding plane failure with respect to the stress distribution, thus enhancing the connection of cracks from the flaw and bedding planes.

For specimens containing anti-dip flaws, the bedding planes penetrating the flaw are fractured by a combination of the shear and tensile stresses. Bedding-plane sliding fractures propagate with multiple vertical tensile cracks initiating from bedding planes. It can be concluded from the experimental observations that these tensile cracks have a weakening effect on the rock properties. Compared to pro-dip flaws, the anti-dip flaws have a greater impact on the distribution of stress within bedded rocks. The flaw provides a free boundary for penetrating bedding planes; hence, compression-induced tensile cracks are able to propagate along the bedding planes.

5.4. Implication for the rock slope

Controlled laboratory studies of fracture evolution in bedded rock allow the impact of individual influences of bedding and flaw orientations relative to the stress field to be deconvolved from other obscuring factors such as heterogeneities, scale influences and the presence of non-uniform stress fields. Such studies are of significance to engineering practice in defining the failure modes in slopes and underground excavations where failure typically occurs both on fractures and through intact rock (Wu et al., 2004; Do et al., 2017). In the following, we use a bedded rock slope as an example to explain the implication of the experimental results.

5.4.1. Failure modes of bedded rock slope

The bedding orientation dominates the failure mode of bedded rock specimens as well as rock slopes. Fig. 17 illustrates a comparison of failure mechanisms between rock specimens and model slopes with various bedding inclinations. The generated fractures are prominently marked on both the images of specimens and the slope profiles.

The behavior of a specimen containing horizontal bedding planes predicts the deformation of a slope containing gently inclined strata (Fig. 17 (a)). The orientations of the maximum and minimum principal stresses within the slope are sub-vertical and sub-horizontal, respectively. Driven by gravity, the slope slowly displaces downwards along the weak intercalated rock layer with multiple vertical tensile cracks developing to accommodate this deformation (Fan et al., 2009). This type of slope commonly has several sliding blocks separated by deep tensile-induced grooves.

The rock specimen with $\alpha = 60^\circ$ responds similarly to a steeply-bedded slope containing pro-dip bedding planes (Fig. 17 (b)). Shear sliding occurs along the bedding plane in both the specimen and slope. Note that fractures in real slopes are typically more complicated than those marked on the sketch – these effects of increased complexity are discussed later.

Buckling failure occurs in the bedded rock slopes where the maximum principal stress is sub-parallel to the bedding plane, as shown in Fig. 17 (c). Long and slender rock columns with their bases fixed tend to flex downwards. When the flex-induced tensile stress exceeds tensile strength of rock, buckling failure occurs.

For rock slopes containing anti-dip bedding planes as shown in Fig. 17 (d), the local tensile cracks those are parallel to the slope surface are the first to initiate under the action of gravity. These tensile cracks are connected by rock bridges those are subjected to shear force. As the cracks extend across the bridges, the mass fails and the slope finally slides along a potential sliding surface. This process is similar to the response of a specimen with $\alpha = 30^\circ$.

5.4.2. Fracture evolution in bedded rock slope

The failure of rock slopes containing rock bridges typically originates from the extension of pre-existing structural flaws to disrupt these bridges. Fracture evolution processes are diverse and are influenced by the orientation, scale and distribution of structural flaws. We can predict the fracture evolution in bedded rock slope according to our experimental results. Fig. 18 illustrates the prediction of a pro-dip slope containing differently inclined structural flaws.

The structural flaw in Fig. 18 (a) is pro-dip to the bedding plane with a shallower inclination than the bedding plane. Tensile cracks initiating from the flaw extend both upwards and downwards. The lower tensile crack transforms into a bedding sliding fracture while the upper one remains tensile nature with only minor shear sliding components. The inclination of the structural flaw in Fig. 18 (b) is steeper than that of the bedding plane. After tensile cracks initiate from the flaw tips, a stepped fracture consisting of bedding sliding fractures and interlayer tensile cracks gradually extend toward the surface of the slope. The structural flaw in Fig. 18 (c) is anti-dip to the bedding plane. Contrary to the former two conditions, multiple bedding fractures and tensile cracks are generated in this slope with these fractures densely distributed and forming a network.

6. Summary and conclusions

This paper presents an experimental study of fracture evolution in artificial bedded rocks containing single structural flaws. The specimens are fabricated to include various bedding and flaw inclinations and are then tested under uniaxial compression. Cracking patterns and stress-strain data are recorded during the entire loading process. The testing results are summarized as follows.

6.1. Stress and strain

All stress-strain curves show four phases representing the entire

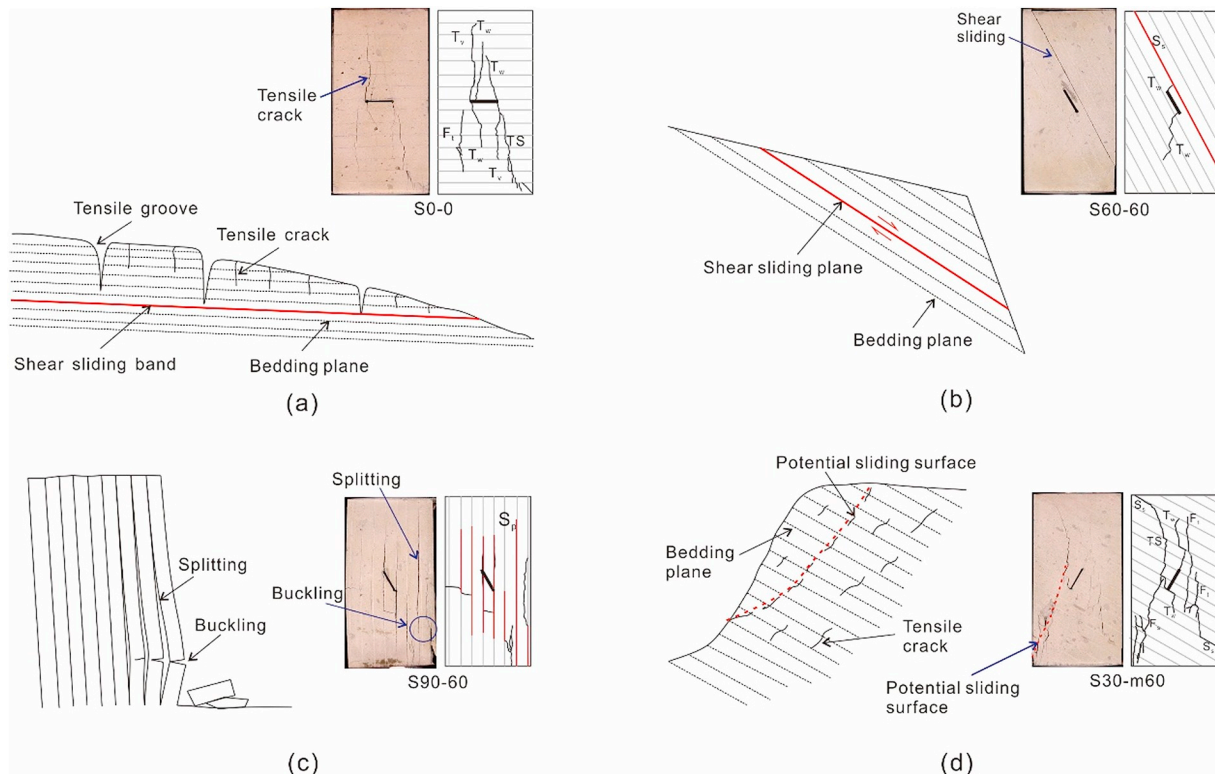


Fig. 17. Comparison of failure mechanisms between bedded rock slopes and specimens with different bedding inclinations. (a) Gently inclined, (b) pro-dip, (c) sub-vertical, and (d) anti-dip geometries.

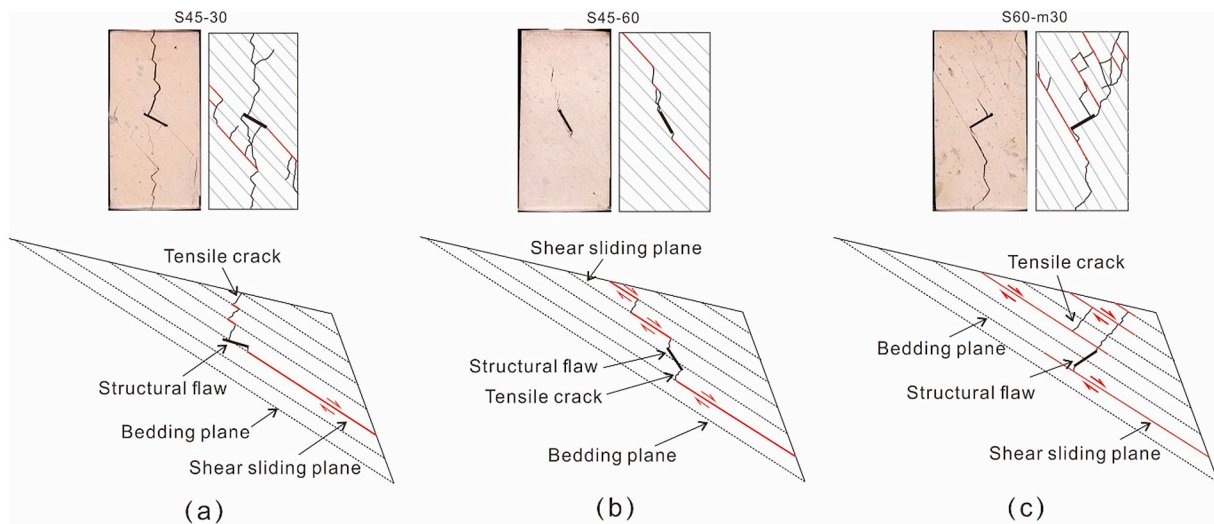


Fig. 18. Fracture evolution in pro-dip slopes containing a structural flaw. (a) pro-dip flaw with shallower inclination than bedding, (b) pro-dip flaw with steeper inclination than bedding, and (c) anti-dip flaw.

deformation process. These can be characterized as four deformation types, namely, ductile with fluctuation, ductile without post-peak fluctuation, brittle failure with fluctuation and brittle failure without post-peak fluctuation. These curve types transform in the above order as bedding planes become steeper.

Mechanical parameters (i.e. σ_c , ε_c and E) are derived on the basis of the stress-strain data. σ_c and ε_c appear to vary similarly versus bedding inclination, which first show decreasing trends and then increase as the bedding plane becomes steeper. However, E has a positive relation to the increased bedding plane inclination in general.

6.2. Crack and failure

Nine crack types are identified from the recorded images of the fractured specimens, in which bedding sliding and splitting are potentially newfound failure modes in such models, compared to previous homogeneous rock tests. These cracks have non-planar paths with a few transitions when they approach bedding planes.

The inclination of the bedding plane exerts a significant effect on crack initiation and propagation in artificial bedded rocks.

- The tensile wing crack propagates as the primary crack in most low-inclined bedded specimens, but initiates along with other crack types in steeply-bedded specimens.
- With an increase of the bedding inclination, the tensile crack initiating from the flaw more likely propagates along bedding planes and may result in the failure along the entire bedding plane. However, as the bedding inclination approaches 90° , the failure transforms from sliding to splitting. The accumulative length of the bedding fractures has a positive relation to bedding inclination regardless of the variation in the flaw inclination.
- In the pro-dip flaw tests, tensile cracks mostly initiate from the structural flaw and bedding fractures are triggered by shear stress. But in the anti-dip flaw tests, many tensile cracks initiate from bedding planes in addition to structural flaw and the resulting crack density is much higher. Bedding fractures typically develop under the combined action of the shear and tensile stress.
- The failure mode in the bedded specimens transforms from the pure tensile mode to the combined tensile-bedding sliding mode and subsequently to the bedding splitting mode as the bedding planes steepen.
- The experimental results are significant for the analysis of bedded rock slopes. The failure modes and fracture evolution processes of

rock slopes containing different bedding planes and structural flaws can be predicted on the basis the observed fracture patterns in specimens.

Acknowledgments

This research was funded by the National Key R&D Program of China (Grant No. 2017YFC1501305) and the Key Program of National Science Foundation of China (Grant No. 41230637). This financial support is appreciated. We are also grateful to Dr. Peiwu Shen, Dr. Lei Huang and Dr. Xuexue Su for assisting in the experiments.

References

- Bandis, S., Lumsden, A.C., Barton, N.R., 1981. Experimental studies of scale effects on the shear behaviour of rock joints. *Inter. j. of rock mech. and mining sci. & geomechanics abstracts* 18 (1), 1–21.
- Barton, N., Quadros, E., 2015. Anisotropy is everywhere, to see, to measure, and to model. *Rock Mech. Rock. Eng.* 48 (4), 1323–1339.
- Bobet, A., Einstein, H.H., 1998. Fracture coalescence in rock-type materials under uniaxial and biaxial compression. *Int. J. Rock Mech. Min. Sci.* 35 (7), 863–888.
- Cai, M., Kaiser, P.K., 2004. Numerical simulation of the Brazilian test and the tensile strength of anisotropic rocks and rocks with pre-existing cracks. *Int. J. Rock Mech. Min. Sci.* 41, 478–483.
- Cao, P., Liu, T., Pu, C., Lin, H., 2015. Crack propagation and coalescence of brittle rock-like specimens with pre-existing cracks in compression. *Eng. Geol.* 187, 113–121.
- Cao, R.H., Cao, P., Lin, H., Pu, C.Z., Ou, K., 2016. Mechanical behavior of brittle rock-like specimens with pre-existing fissures under uniaxial loading: experimental studies and particle mechanics approach. *Rock Mech. Rock. Eng.* 49 (3), 763–783.
- Carpinteri, A., Paggi, M., 2008. Size-scale effects on strength, friction and fracture energy of faults: a unified interpretation according to fractal geometry. *Rock Mech. Rock. Eng.* 41 (5), 735–746.
- Chen, C.H., Chen, C.S., Wu, J.H., 2008. Fracture toughness analysis on cracked ring disks of anisotropic rock. *Rock Mech. Rock. Eng.* 41 (4), 539–562.
- Cheng, Y., Wong, L.N.Y., Zou, C., 2015. Experimental study on the formation of faults from en-echelon fractures in Carrara marble. *Eng. Geol.* 195, 312–326.
- Do, T.N., Wu, J.H., Lin, H.M., 2017. Investigation of Sloped Surface Subsidence during Inclined Seam Extraction in a Jointed Rock Mass Using Discontinuous Deformation Analysis. *Inter. J. of Geomech.* 17 (8).
- Duveau, G., Shao, J.F., Henry, J.P., 1998. Assessment of some failure criteria for strongly anisotropic geomaterials. *Mech. Cohes. Frict. Mat.* 3 (1), 1–26.
- Fan, X.M., Xu, Q., Zhang, Z.Y., Meng, D.S., Tang, R., 2009. The genetic mechanism of a translational landslide. *Bullet. of Eng. Geol. & the Env.* 68 (2), 231–244.
- Feng, X.T., Ding, W., Zhang, D., 2009. Multi-crack interaction in limestone subject to stress and flow of chemical solutions. *Int. J. Rock Mech. Min. Sci.* 46 (1), 159–171.
- Gholami, R., Rasouli, V., 2014. Mechanical and elastic properties of transversely isotropic slate. *Rock Mech. Rock. Eng.* 47 (5), 1763–1773.
- Goodman, R.E., 1989. *Introduction to Rock Mechanics*. Wiley, New York.
- Hoek, E., Bray, J.D., 1981. *Rock Slope Engineering*. CRC Press, Boca Raton.
- Indelicato, F., Paggi, M., 2008. Specimen shape and the problem of contact in the assessment of concrete compressive strength. *Materials and Structures* 41 (2), 431.
- Morgan, S.P., Einstein, H.H., 2017. Cracking processes affected by bedding planes in

- Opalinus shale with flaw pairs. *Eng. Fract. Mech.* 176, 213–234.
- Niandou, H., Shao, J.F., Henry, J.P., Fourmaintraux, D., 1997. Laboratory investigation of the mechanical behaviour of Tournemire shale. *Int. J. Rock Mech. Min. Sci.* 34 (1), 3–16.
- Tang, H., Huang, L., Juang, C.H., Zhang, J., 2017. Optimizing the Terzaghi Estimator of the 3D distribution of rock fracture orientations. *Rock Mech. Rock. Eng.* 50 (8), 2085–2099.
- Tien, Y.M., Kuo, M.C., Juang, C.H., 2006. An experimental investigation of the failure mechanism of simulated transversely isotropic rocks. *Int. J. Rock Mech. Min. Sci.* 43 (8), 1163–1181.
- Togashi, Y., Kikumoto, M., Tani, K., 2017. An experimental method to determine the elastic properties of transversely isotropic rocks by a single triaxial test. *Rock Mech. Rock. Eng.* 50 (1), 1–15.
- Wong, L.N.Y., 2008. Crack Coalescence in Molded Gypsum and Carrara Marble. Degree Thesis. Massachusetts Institute of Technology.
- Wong, L.N.Y., Einstein, H.H., 2009a. Systematic evaluation of cracking behavior in specimens containing single flaws under uniaxial compression. *Int. J. Rock Mech. Min. Sci.* 46 (2), 239–249.
- Wong, L.N.Y., Einstein, H.H., 2009b. Crack coalescence in molded gypsum and Carrara marble: part 1. Macroscopic observations and interpretation. *Rock Mech. Rock. Eng.* 42 (3), 475–511.
- Wong, L.N.Y., Einstein, H.H., 2009c. Crack coalescence in molded gypsum and Carrara marble: part 2—microscopic observations and interpretation. *Rock Mech. Rock. Eng.* 42 (3), 513–545.
- Wong, R.H.C., Chau, K.T., Tang, C.A., Lin, P., 2001. Analysis of crack coalescence in rock-like materials containing three flaws—part I: experimental approach. *Int. J. Rock Mech. Min. Sci.* 38 (7), 909–924.
- Wu, J.H., Ohnishi, Y., Nishiyama, S., 2004. Simulation of the mechanical behavior of inclined jointed rock masses during tunnel construction using discontinuous deformation analysis (DDA). *Inter. J. of Rock Mech. & Mining Sci.* 41 (5), 731–743.
- Yang, S.Q., Huang, Y.H., 2017. An experimental study on deformation and failure mechanical behavior of granite containing a single fissure under different confining pressures. *Environ. Earth Sci.* 76 (10), 364.
- Yang, S.Q., Jing, H.W., 2011. Strength failure and crack coalescence behavior of brittle sandstone samples containing a single fissure under uniaxial compression. *Int. J. Fract.* 168 (2), 227–250.
- Yang, S.Q., Yang, D.S., Jing, H.W., Li, Y.H., Wang, S.Y., 2012. An experimental study of the fracture coalescence behaviour of brittle sandstone specimens containing three fissures. *Rock Mech. Rock. Eng.* 45 (4), 563–582.
- Yang, S.Q., Liu, X.R., Jing, H.W., 2013. Experimental investigation on fracture coalescence behavior of red sandstone containing two unparallel fissures under uniaxial compression. *Int. J. Rock Mech. Min. Sci.* 63, 82–92.
- Yang, S.Q., Huang, Y.H., Tian, W.L., Zhu, J.B., 2017a. An experimental investigation on strength, deformation and crack evolution behavior of sandstone containing two oval flaws under uniaxial compression. *Eng. Geol.* 217, 35–48.
- Yang, X.X., Jing, H.W., Tang, C.A., Yang, S.Q., 2017b. Effect of parallel joint interaction on mechanical behavior of jointed rock mass models. *Int. J. Rock Mech. Min. Sci.* 92, 40–53.
- Zou, C., Wong, L.N.Y., 2014. Experimental studies on cracking processes and failure in marble under dynamic loading. *Eng. Geol.* 173, 19–31.
- Zou, C., Wong, L.N.Y., Loo, J.J., Gan, B.S., 2016. Different mechanical and cracking behaviors of single-flawed brittle gypsum specimens under dynamic and quasi-static loadings. *Eng. Geol.* 201, 71–84.